PSI-Bericht Nr. 23
Dezember 1988

Paul Scherrer Institut

Labor für Materialwissenschaften

PIREX II
A New Irradiation Facility for Testing Fusion First Wall Materials

P. Marmy, M. Daum, D. Gavillet, S. Green, W.V. Green,
F. Hegedus, S. Proennecke, U. Rohrer, U. Stiefel,
M. Victoria

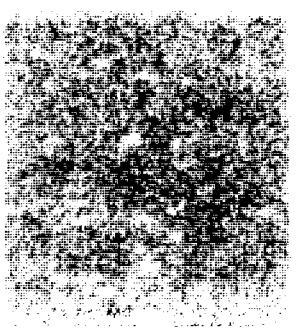

Paul Scherrer Institut
Würenlingen und Villigen
CH-5232 Villigen PSI

Telefon 056/99 21 11
Telex 82 74 14 psi ch
Telefax 056/98 23 27 PSI CH

PSI - Bericht Nr. 23

PIREX II

A New Irradiation Facility for Testing Fusion First Wall Materials

P. Marmy, M. Daum, D. Gavillet, S. Green, W.V. Green, F. Hegedus,
S. Proennecke, U. Rohrer, U. Stiefel, M. Victoria

Dezember 1988

Formerly EIR/SIN

CH-5232 Villigen PSI
Switzerland

PAUL SCHERRER INSTITUTE

13.12.88

* PIREX II

A New Irradiation Facility for Testing Fusion First Wall Materials

P. Marmy, M. Daum, D. Gavillet, S. Green, W.V. Green, F. Heiedus, S. Proennecke, U. Rohrer, U. Stiefel, and M. Victoria

Abstract

A new irradiation facility, PIREX II, became operational in March 1987. It is located on a dedicated beam line split from the main beam of the 590 MeV proton accelerator at the Paul Scherrer Institute (PSI). Irradiation with protons of this energy introduces simultaneously displacement damage, helium and other impurities. Because of the penetration range of 590 MeV protons, both damage and impurities are homogeneously distributed in the target material.

The installation has its own beam line optics that can support a proton current of up to 50 μA. At a typical beam density of 4 $\mu A/mm^2$, the damage rate in steels is 0.7 x 10^{-5} dpa/sec (dpa: displacements per atom) and the helium production rate is 170 appm He/dpa. Both flat tensile specimens of up to 0.4 mm thickness and tubular fatigue samples of 3 mm diameter can be irradiated. Cooling of the sample is performed by flowing pressurized helium gas over the sample. Irradiation temperatures can be controlled between 100^0 and 800^0 C. Installation of an *in situ* low cycle fatigue device is foreseen.

Beams of up to 20 μA have been obtained, the beam having approximately a gaussian distribution of elliptical cross section with 4 σ between 0.8 and 3 mm by 10 mm.

Irradiations for a dosimetry program have been completed on samples of Al, Cu, Fe, Ni, Au, W, and the 1.4914 ferritic steel. The evaluation of results allows the correct choice of reactions to be used for determining total dose, from the standpoint of half life and gamma energy.

A program of irradiations on candidate materials for the Next European Torus (NET) design (Cu and Cu alloys, the 1.4914 ferritic martensitic steel, W and W-Re alloys and Mo alloys), where the above mentioned characteristics of this type of irradiation can be used advantageously, is now under way.

* PROTON IRRADIATION EXPERIMENT

PIREX II
A New Irradiation Facility for Testing Fusion First Wall Materials

1. Introduction

The first wall of a fusion reactor will undergo radiation damage from a neutron spectra with a maximum at an energy of 14 MeV. This type of energetic radiation introduces simultaneously both displacement damage and impurities produced through nuclear reactions. Of particular importance are the gaseous impurities, helium and hydrogen, since they give rise to microstructural changes, such as bubbles and to substantial modifications of properties, as is the case with the embrittlement of the irradiated material.

The studies and accelerated tests of materials irradiated with this type of neutron spectra are faced with the problem that no irradiation source of sufficient intensity is available at present. Correlations are made with either fission neutrons or charged particle irradiations.

Since the late seventies, medium energy protons have been used in both the LAMPF accelerator in Los Alamos, U.S.A. and the machine available in the Paul Scherrer Institute (PSI, previously SIN/EIR). Irradiations with protons in the energy range of these accelerators (600 - 800 MeV), introduces helium and other impurities through spallation reactions, as well as displacements cascades.

In the machine at the PSI, an irradiation facility, PIREX I, was used to test the feasibility of such an irradiation method to simulate fusion neutron damage. On the basis of the initial results, a second installation, PIREX II, was built and started operating in March 1987. The present paper describes its characteristics and reviews some of the early results obtained.

2. The PIREX I Facility

The PIREX I facility has been described in detail elsewhere [1]. About sixty aluminium and aluminium alloy targets were irradiated to doses up to 6 dpa and irradiation temperatures between 370 K and 870 K. The main results obtained are as follows:

- Helium is produced at a measured rate of 255 appm/dpa [1].
- Different void distributions are observed for irradiation temperatures up to 410 K [2,3]. Their average size is 83 nm at 410 K and 5 dpa.

- Helium bubbles are observed at irradiation temperatures from 390 K upwards. Two regions can be described as a function of the irradiation temperature. In the lower temperature region (390 - 550 K), there is little variation in the size (from 2.5 nm up to 7.5 nm diameter), while their density remains around $5 \cdot 10^{22}$ m^{-3} [1,4,5]. The bubble structure is nucleation controlled in this region. At temperatures above 550 K, bubbles grow to much larger sizes (i.e., 85 nm diameter at 700 K [3]). The microstructural observations and the stability of the microstructure have been confirmed by additional observations using electrical resistivity [6], neutron and X-ray scattering [7] and positron annihilation [8,9].

- The post irradiation tensile properties of pure aluminium [10-12] show irradiation hardening, the flow stress depending on the square root of the dose for all testing temperatures in the range from 190 K to 473 K. The hardening is independent of the bubble structure and has been explained by the presence of submicroscopic clusters of transmutation atoms or stabilized by them. This last result demonstrates the need of producing first wall related information using radiation sources were the correct characteristics of the damage with high energy neutrons are reproduced.

3. Calculations

The calculations of nuclear interactions by the 590 MeV protons are made with a modified version of the High Energy Transport Code (HETC) [13]. Previous calculations for a number of targets were produced [14] using the Nucleon Meson Transport Code (NMTC) are less accurate for helium production. The interaction of the proton with a target atom is described by the intranuclear cascade-evaporation model as reported by Serber [15]. The associated wavelength of a 590 MeV proton is sufficiently short that the interaction takes place with the individual nucleons rather than with the nucleus as a whole. During this intranuclear cascade process, a number of protons and neutrons escape the nucleus. The nucleus is left in a highly excited state, which decays to the ground state by the emission of protons, neutrons, deuterons, tritons and ^{3}He and ^{4}He. These evaporated particles are emitted isotropically, with an energy of a few MeV. This is the origin of the helium and hydrogen production that is uniformly distributed in the thickness of the target and simulates the nuclear effects of the 14 MeV neutron spectra.

HETC calculates the type, energy, location and direction of all particles produced by each interaction. Cascade nucleons with energies higher than 20 MeV are transported and may produce further interactions before they leave the material. A treatment for fission events is included in the calculation.

The resultant nucleus loses energy inelastically by electronic excitations and elastically by atomic collisions, which produce the atomic displacement cascades. A recoil energy distribution is obtained. The formulation by Robinson [16] of the

Table I
Summary of Medium Energy Proton Irradiation Damage Parameters
from Ref. [20]

		Al	Fe	Ni	Cu	Mo	W	Au
Damage Energy Cross	590 MeV	50	280	-	317	704	1533	1728
Sections (bkeV)	750 MeV	49	298	339	378	761	1743	2017
Average Recoil Energy	590 MeV	3.0	2.4	-	-	2.0	3.4	6.5
(MeV)	750 MeV	3.3	2.6	2.6	2.5	2.3	4.2	7.6
Average Damage Energy	590 MeV	87	269	-	326	481	658	749
(keV)	750 MeV	83	263	293	307	468	722	786
Displacement Threshold (eV)		17	40	40	30	60	90	35
He/dpa Ratio (appm He per dpa)								
HETC Calculated	590 MeV	330	172	-	126	186	245	86
HETC Measured	590 MeV	215 (255*)						
HETC Measured	750 MeV	290	169	158	102	125	98	30
HETC Calculated	750 MeV	386	192	180	121	217	272	97

*Thin Sample Corrected for Recoil Losses

model of Lindhard et al. [17] is used to determine the partition between electronic excitation and displacement damage. The damage energy so obtained is then combined with the production cross sections for each isotope, to give the total damage energy cross section. A modified Kinchin-Pease model is then assumed to relate the displacements per atom (dpa) to the proton fluence. The calculated damage characteristics for a number of materials are shown in Table I.

Note that the damage energy is much less than the recoil energy. This energy difference appears as heat. However, this represents only 1 % of the total heat production which comes from proton-electron interactions.

Table II
Comparison of the Relevant Impurities Produced in
Ferritic Steel 1.4914 under 590 MeV Protons and Fusion Neutrons

Element	Impurity production in appm/dpa	
	590 MeV protons	fusion neutrons (+)
Co	2.6	0.7
Fe	-266 ($)	-51 ($)
Mn	66	38
Cr	12	0.5
V	38	12
Ti	32	1.5
Si	7	-1
Al	2.7	0.5
S	12	-0.02
P	8	0.004
C	0.2	-0.3
He	195	19
H	956 (*)	70
Sc, Ca, K, Ar, Cl	81	N/A

(*) Because of the high energy processes involved, most of it will escape the specimen
($) There is a net decrease of the iron atoms
(+) Mean production after 1 year of exposure

A listing of the impurities produced in ferritic steel without any decay consideration is given in the left column of Table II. The right column shows the impurities produced by a typical fusion spectrum [18]. The He produced by the protons is too high by a factor of eight, but a part of it is not retained in the thickness of the target material as it is produced with a high recoil energy. This could give a different material response, especially under fatigue at high temperatures. Despite the very low production rate, the other solid irradiation products could influence the mechanical properties, especially at very high doses.

4. Description of the PIREX II Facility

The design of the new proton facility was made with a number of objectives in mind. Specimen size was maximized, compatible with the cooling conditions that could be attained with adequate temperature control and the radioactivity produced by the irradiation of the target. The flexibility needed in the beam density on the target specimen plane implied independent control of the beam line or a dedicated beam line. Furthermore, at the end of an irradiation, the change of the irradiated specimen should be performed without interfering with other accelerator users and with sufficient radiological protection for the operators.

4.1 The Beam Line

Given the above conditions, the decision was made to build a new beam line. A partial view of the distribution of the accelerator beam is shown in Fig. 1(a). An intense proton beam ($\approx$ 300 μA at present) is extracted at 590 MeV from the isochronous ring cyclotron. An electrostatic septum splits off part of this beam, at a maximum intensity of 50 μA. This beam is directed towards a biomedical facility (BMA) or, by switching off the last bending magnet, to the PIREX station.

The beam line at PIREX, Fig. 1 (b), has been designed so that beam size and position can be measured, controlled and stabilized remotely, such that for a variety of target specimen geometries, an average luminosity of 4 $\mu A \cdot mm^{-2}$ can be attained. A double quadrupole system (QCA1, QCA2, QCB3, QCB4) focuses the beam in the specimen plane. Its position in both horizontal and vertical axes is defined by two sets of steering magnets (SCB1X, SCB2Y, SCB3X, SCB4Y). The size of the beam and its position can be controlled with a precision of 0,1 mm by using special profile and center-of-gravity monitors (MCP and MCS 1 to 14). In addition, the beam luminosity at the target can be controlled by a beam spill monitor (AGOC).

The resulting beam has an approximately gaussian profile. Intensities up to 20 μA have been produced with 4 σ values between 0,8 and 3.5 mm on the horizontal axis by up to 10 mm on the vertical axis. Typical beam profiles at the plane of the target are shown in Fig. 2. They were measured from autoradiographs of irradiated targets and correspond therefore to an accumulated beam size. The example shown in the figure was produced by a one-hour irradiation. A constant damage deposition can be obtained by moving the beam around the center position. An automatic beam wobbler displaces the beam linearly with time. For this purpose a number of computer programs have been adapted or developed to control the beam. Beam transport calculations, based on measurements of the control monitors, give the beam size and geometry or the magnet settings to produce given beam dimensions. The beam centering and beam positioning in the target is controlled by standard software.

Fig. 1
Beam Line PIREX I
The overview of the installation is shown in (a) and the specific beam components of PIREX are shown in (b).

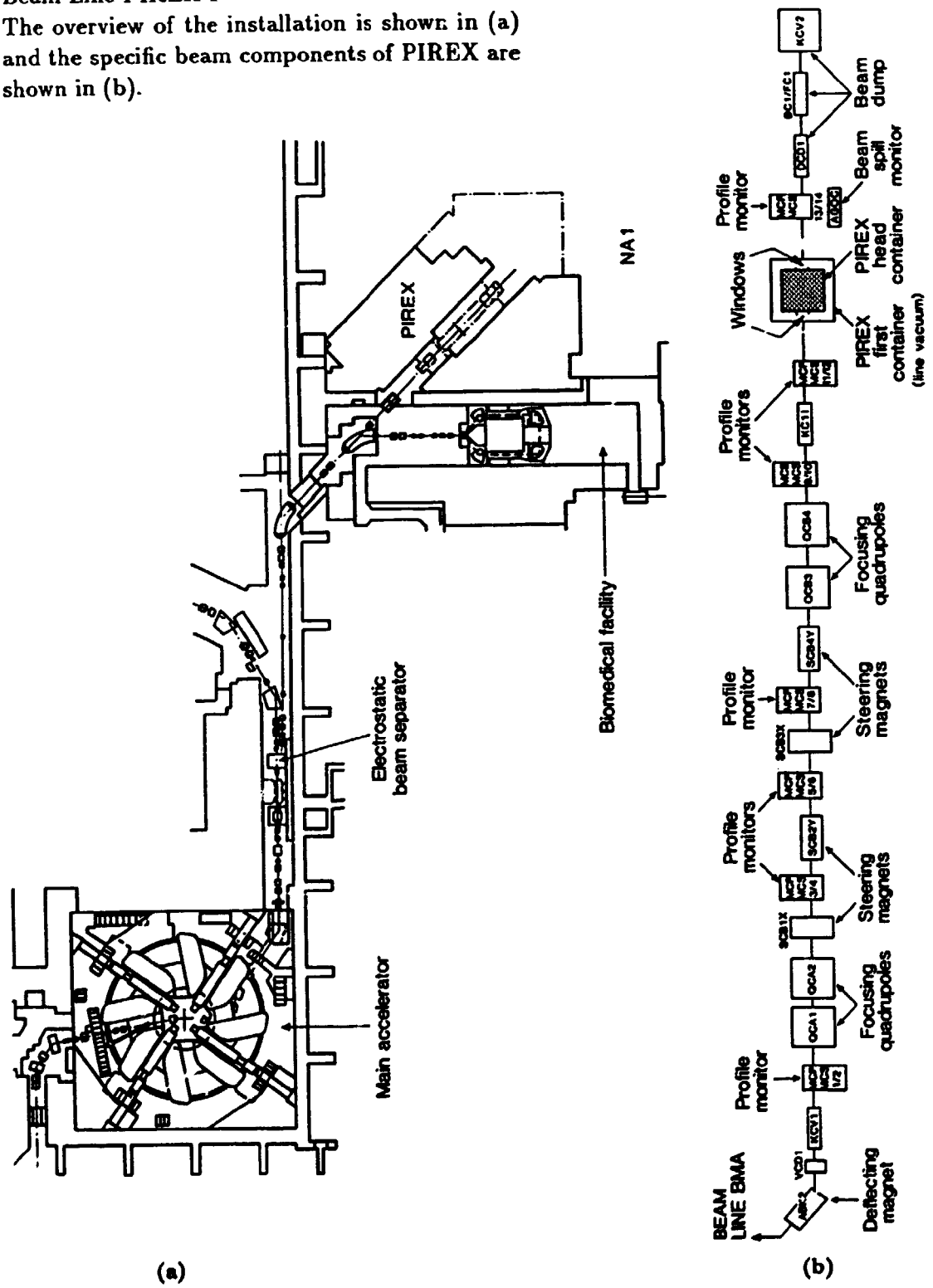

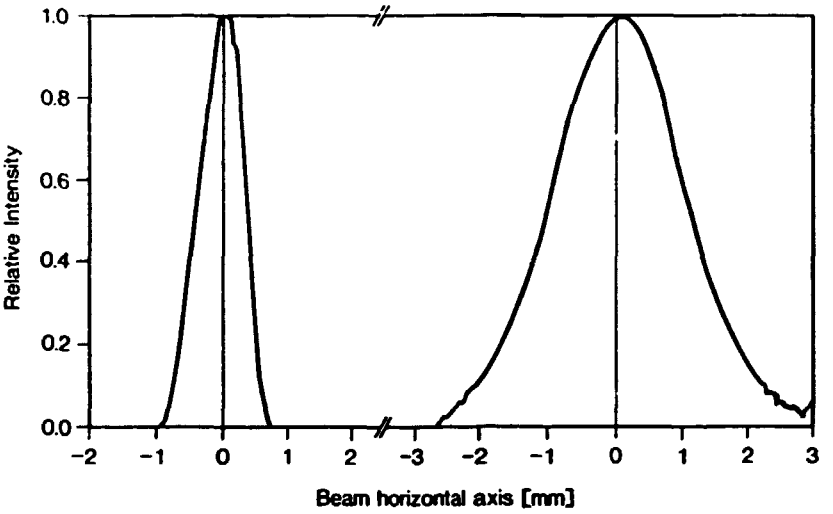

Fig. 2
Typical beam profiles

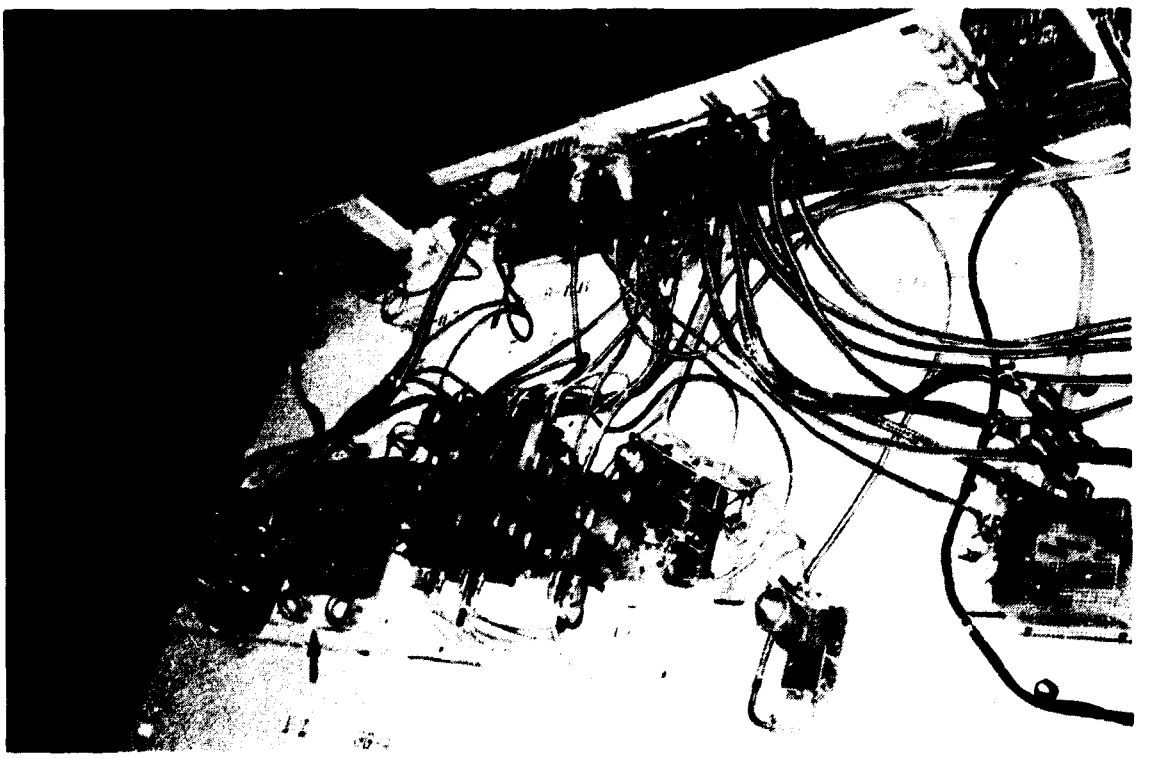

Fig. 3
Upper view of the PIREX facility. The PIREX location is indicated by an arrow.

The irradiation head is inserted vertically into a double wall vacuum container isolated from the beam line vacuum. The beam is transported through aluminium windows, 100 μm thick. A beam dump is placed immediately behind the target, which allows the beam spreading to be tolerated without interference with other experiments. The beam line is surrounded by 3,5 m of local iron shielding. A general view of the upper part of the facility can be seen in Fig. 3.

4.2 Irradiation Head and Specimen Geometry

A large amount of heat, between 2000 and 11000 Watts·cm^{-3} depending on the target material, is deposited in the volume of the irradiated specimen by the proton beam. One of the main problems encountered in using this type of irradiation is therefore the cooling of the specimen. In the PIREX installation this problem is solved by using helium gas under pressure as the cooling medium.

The general structure of the irradiation head and specimen area is shown schematically in Fig. 4, and in its actual construction, in Fig. 5. The helium gas circulates at pressures of up to 50 bars and its temperature is regulated by a 29 kW counterflow heat exchanger that cools the gas as it exits the specimen region and a 9 kW electrical heater that preheats the input gas.

A biological shield is located in the upper region of the irradiation head. In the uppermost region, after the vacuum flange, a mechanical device operates as a switch for all electrical, gas and vacuum connections from the head to the exterior and as well as a clamp holder to the transport shielding bottle. All connections can be disconnected remotely. In Fig. 6 a general view of this mechanism can be seen.

Two types of samples have been chosen, a flat plate tensile specimen and a thin walled tubular specimen for low cycle fatigue tests, see Fig. 7. Typical wall or plate thickness is 0.34 mm for a ferritic steel target.

The specimen is enclosed in a cooling tube, see Fig. 8. Helium gas is circulated at a pressure up to 50 bar inside this tube, with the specimen placed coaxially in it. Because the beam size is defined by the geometry of the specimen target, the cooling tube is heated by the beam only partially around its circumference. This introduces a thermal gradient and therefore, thermal stresses. A hoop stress is also present because of the internal gas pressure. Because of changes in the beam intensity, the cooling tube will be fatigued under these stresses. Inconel X-750, working at about one half its yield stress at the highest irradiation temperature, has been chosen as material for this tube. Another design uses Ti-Al-4V as material to reduce the activation, and allows a maximum pressure of 40 bar. This cooling tube has been in operation for 1000 irradiation hours.

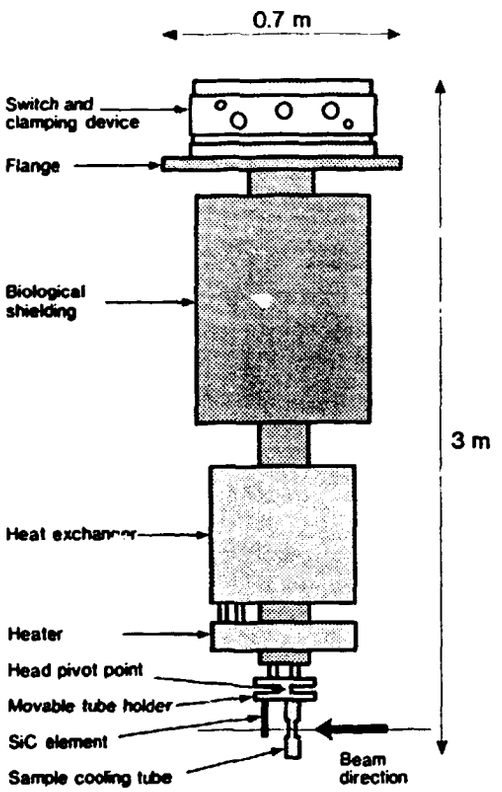

Fig. 4
Schematical drawing of the PIREX irradiation head

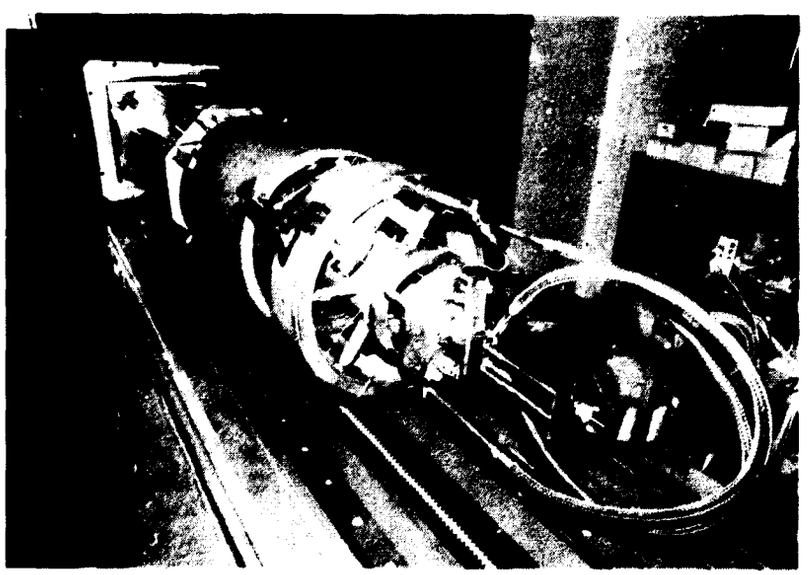

Fig. 5
View of the PIREX irradiation head

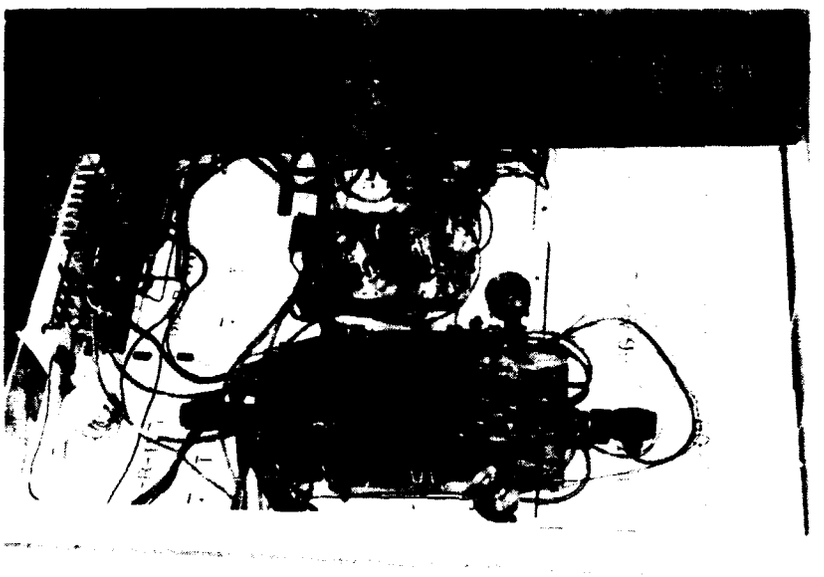

Fig. 6
View of the automatic coupling device. The center part is the clamp to pull up the head.

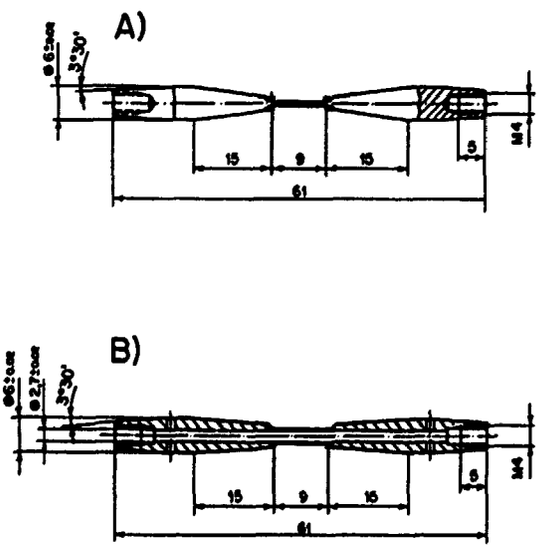

Fig. 7
Drawing of the tensile specimen (A) and of the fatigue specimen (B)

The same cooling system is used in a second irradiation head that can irradiate three specimens simultaneously. Each specimen is placed in a separate cooling tube and the three are connected in series in the cooling gas stream. This system is shown in Fig. 9. This configuration is possible due to the high penetration power of the 590 MeV proton beam.

A SiC pointed element is placed behind the specimen and serves both as a beam detector and centering device. It is precisely positioned parallel to the tube axis. The specimen tube and manifold can be rotated out of the beam through a pivot point shown in Fig. 8. The beam can then be aligned on the horizontal plane by using the SiC element which provides both a temperature signal and a scattered beam which is detected by the beam spill monitor. Optimizing both signals aligns the beam with the SiC element and therefore with the target specimen. A new beam detector using thin thermocouples is now under development.

As is described in section 5, the radioactivities present after irradiation are high and they can be only managed conveniently in a hot cell. A shielded transport bottle is used to move the irradiation head and irradiated specimen, see Fig. 10. It is made of steel walls of 150 mm thickness and weights 18 tons. It is furnished with a motor driven clamp system, with remote controls, that can hold the irradiation head and extract it from the vacuum bottle. The irradiation head with the irradiated specimen is then moved to the hot cell in the transport bottle, were the specimen is removed and replaced by a new one, see Fig. 11.

4.3 The Helium Cooling Loop and the Irradiation Temperature Determination

A stream of helium gas is used to cool the specimen. It is provided by a gas loop in which the flow rate is controllable between 5 and 15 $g \cdot sec^{-1}$, the gas pressure can be controlled between 11 and 51 bars. Gas velocity is 120 $m \cdot sec^{-1}$ or less. The energy loss of the 590 MeV protons in the gas is insignificant and the gas temperature increases only a few degrees as it extracts the heat deposited in the specimen. It can extract up to approximately 150 $W \cdot/cm^2$.

A series of parametric thermohydraulic simulation experiments were performed [19] in which the specimen was heated by ohmic heating, and a series of thermocouples measured the specimen temperature and that of the gas input and output. Other variables such as pressures and flow rates were also measured. A thermohydraulic correction factor was measured, that allowed the determination of the temperature difference between the surface of the specimen and the gas. The temperature of the specimen is then calculated, for the geometry of the cooling tube and the measured gas parameters, which are constantly monitored and controlled in the gas loop. The irradiation temperature can be controlled to any desired value between 100 and 800^0 C within 20^0 C.

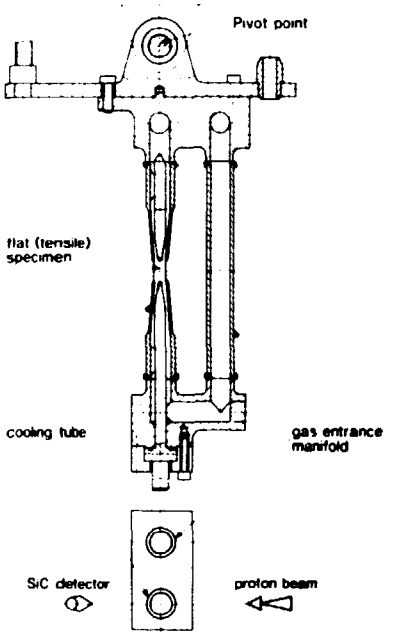

Fig. 8
Drawing of the cooling tube.
Single specimen head.

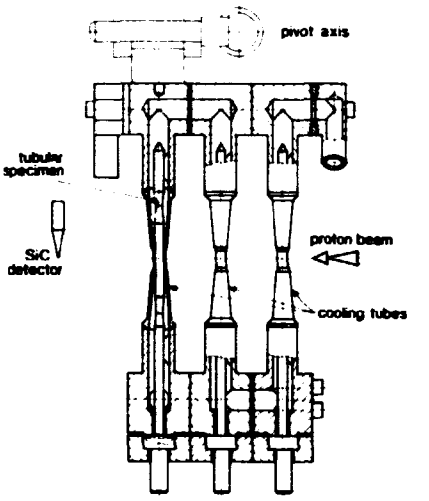

Fig. 9
Irradiation head with three cooling tubes.

Fig. 10
The transport bottle is placed on the target for specimen change.

To check the validity of the calculation, an *in situ* test with a flat specimen was carried out. The specimen was equipped with a 0.2 mm thermocouple mounted in a hole center through the gauge length. In this way the original cooling geometry was fully preserved. In the case of beams with a circular cross section, where the intensity profile is nearly Gaussian, the difference between the calculated and measured values was found to be less than 5^0 C. For other types of beam geometry or for off-center regions of the Gaussian, the largest difference found was 25^0 C.

To prevent surface contamination and corrosion problems, a large gas purifier has been incorporated in the helium gas loop. At full flow, one third of the circulating He gas can be continuously purified; this fraction increases at lower flow rates. The amount of impurities at the exit of the purifier can be reduced to less than 1 ppm in volume for O, H, N and C.

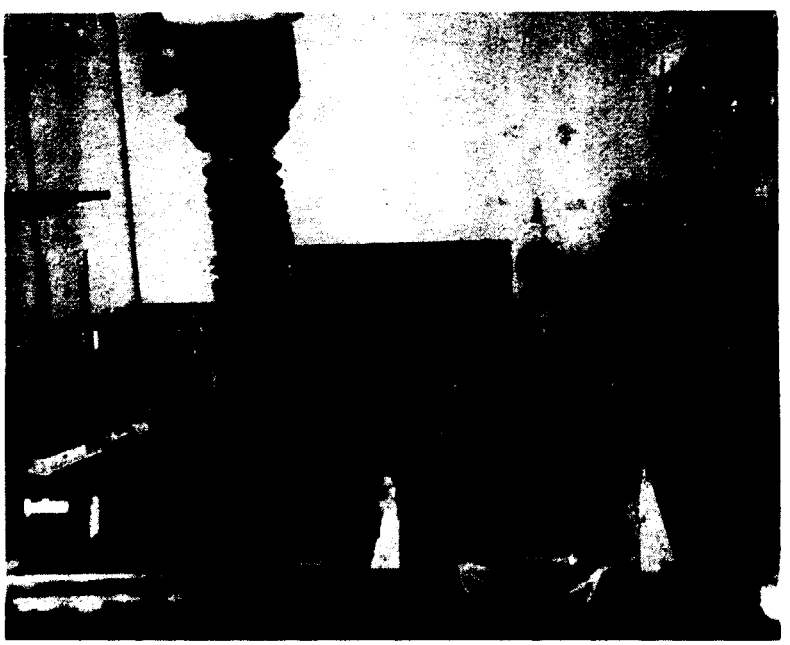

Fig. 11
Specimen change in the hot cell.

5. Initial Experiments

The initial irradiations were performed for dosimetry purposes, on a series of materials that are candidates for later irradiations in the program. These include Cu, Fe, Au, Mo, W, the ferritic 1.4914 steel, and Mo and W based alloys.

In the PIREX I samples, the integrated proton current was measured by means of the ^{27}Al (n,x) ^{22}Na reaction, whose cross section is well known and where the product nuclide has a long half life. The aim of the dosimetry study is to select one or two reactions suitable for a measurement of the proton dose in conditions comparable to those in aluminium. The required characteristics for the reactions are:

- The target nuclide should be a main component of the alloy
- The product nuclide should have a long half life (> 50 days) and should be produced only by a direct reaction
- The measured gamma lines of the product nuclide should be of sufficiently high energy and should not overlap

Irradiations were performed in the above mentioned materials sandwiched with an aluminium foil. The proton doses were determined in the aluminium to calibrate the useful reactions in the other materials.

As an example, Table III shows the long lived isotopes found in 1.4914 steel, of which the original composition is also indicated. The activities measured 38 days after the end of irradiation, total 978.87 $Ci \cdot (g \cdot dpa)^{-1}$. The tubular part of the LCF specimen which is the most highly irradiated, weights 0,18 g, producing a total dose rate at 1 m of 1 R/hour for 1 dpa. As mentioned above, these activities require a hot cell for specimen manipulations. The table shows also that there is considerable lowering (to 11 %) of the calculated activities after a 6 month cooling period. Table IV shows the equivalent results for tungsten.

The Total Reflection X-Ray Scattering (TRTXS) analysing technique is used on separate diluted solutions of the irradiated specimen to determine the yield of the main transmutational products.

As an example, Table III shows the long lived isotopes found in 1.4914 steel, of which the original composition is also indicated. The activities measured 38 days after the end of irradiation, total 978.87 $Ci \cdot (g \cdot dpa)^{-1}$. The tubular part of the LCF specimen which is the most highly irradiated, weights 0,18 g, producing a total dose rate at 1 m of 1 R/hour for 1 dpa. As mentioned above, these activities require a hot cell for specimen manipulations. The table shows also that there is considerable lowering (to 11 %) of the calculated activities after a 6 month cooling period. Table IV shows the equivalent results for tungsten.

The Total Reflection X-Ray Scattering (TRTXS) analysing technique is used on separate diluted solutions of the irradiated specimen to determine the yield of the main transmutational products.

Table III
Long Life Isotope Activity Produced by 590 MeV Protons
in Steel 1.4914 as a Function of the Cooling Time
(other isotopes may influence the long term activity)

Isotopes	Half life	Measured activity 38.6 days after the end of irradiation (mCi/g·dpa)	Calculated activity for the given time after irradiation (mCi/g·dpa)			
			1 month	3 months	6 months	1 year
^{56}Co	78.5	13.41	14.21	8.290	3.700	0.740
^{54}Mn	312.5	75.02	76.12	66.490	54.280	36.230
^{52}Mn	5.6	52.85	119.41	0.063	0.000	0.000
^{51}Cr	27.7	48.98	57.75	12.550	1.271	0.013
^{48}V	16.0	425.60	566.10	40.290	0.765	0.000
^{46}Sc	83.8	137.90	145.60	87.930	41.250	9.140
Unidentified γ-emission at:						
511 keV	$\approx$ 30	225.1	260.00	64.000	8.000	0.200
Total activity:		978.90	1239.20	279.600	109.300	46.300

Table IV
Long Life Isotope Activity Produced by 590 MeV Protons
in Tungsten as a Function of the Cooling Time

Isotopes	Half life (day)	Measured activity 121.1 days after the end of irradiation (mCi/g·dpa)	Calculated activity for the given time after irradiation (mCi/g·dpa)		
			3 months	6 months	1 year
^{175}Hf	70.0	3.87	5.24	2.12	0.35
^{172}Hf	683.0	10.45	10.78	9.82	8.16
^{146}Gd	48.3	4.92	7.63	2.05	0.15
Unidentified γ-emission at:					
271 keV	$\approx$ 800	2.17	2.23	2.06	1.76
306 keV	$\approx$ 800	1.41	1.45	1.34	1.14
665 keV	$\approx$ 30	0.16	0.32	0.04	0.00
791 keV	$\approx$ 25	0.14	0.33	0.03	0.00
1121 keV	$\approx$ 800	1.60	1.64	1.52	1.30
1189 keV	$\approx$ 70	0.66	0.89	0.36	0.06
1230 keV	$\approx$ 800	0.47	0.48	0.44	0.38
Total activity:		25.9	31.00	19.80	13.30

6. Future Program

The PIREX facility had accumulated by October 1988 about 1500 hours of irradiation. It is being used to obtain information on NET candidate materials, in particular the 1.4914 ferritic/martensitic steel which is the alternative candidate for the NET first wall, and a number of tungsten and molybdenum alloys and copper and copper alloys.

Post irradiation mechanical properties (Tensile and Low Cycle Fatigue {LCF}) are being studied in the 1.4914 steel. The main advantage in using PIREX is the helium production rate of 170 appm/dpa in bulk samples, which could only be obtained otherwise in this alloy by helium injection in thin samples or by alloy modifications.

Tungsten, W-Re alloys and Mo and the Mo-base TZM alloy are candidate materials for the heat armour and heat sink components of the divertor design in NET. Both the helium production and the penetration depth of 590 MeV protons are the useful properties of PIREX in this case.

Copper and Cu alloys, which are candidate materials for the cooling components of the divertor are also being irradiated. In this case, PIREX functions as a "users facility" in a contract run by Risø National Laboratory in Denmark.

Apart from these technological applications, a development program of irradiations is taking place simultaneously. It provides the basic radiation damage information needed for the interpretation of PIREX results and the extrapolation to fusion conditions. This program includes post irradiation studies of cascade damage, defect production efficiency, the stability of the microstructure, the nucleation of submicroscopic clusters of defects and impurities and dosimetry studies. Techniques such as high resolution electron microscopy, electrical resistivity, positron annihilation, helium thermal desorption and total reflection X-ray scattering are used as analysing tools.

7. Acknowledgements

The personnel of the Hot Labor at PSI, H.P. Linder, R. Hofer, and A. Christen, assisted in the design of the numerous pieces of equipment that are manipulated in the hot cell. M. Huggenberger and H. Nöthiger designed the thermohydraulic experiment that simulated PIREX cooling conditions and performed the measurements and associated calculations. Additional acknowledgements go to A. Ruede, W. Meier, and R. Obermeier for the general design, to K. Brunner for the construction, and to U. Spillmann, W. Bulgheroni, and M. Emmenmegger for the development of the electronics.

The facility was built with preferential support from EURATOM's Fusion Technology Program. The basic radiation damage physics program is supported by a grant from the Swiss National Research Fund.

References

[1] D. Gavillet, R. Gotthardt, J.L. Martin, S.L. Green, W.V. Green, and M. Victoria; in Effects of Radiation on Materials: Twelfth International Symposium, ASTM STP 870, F.A. Garner, and J.S. Perrin, Eds., 1985, pp. 394 - 406.

[2] B.N Singh, T. Leffers, W.V. Green, and S.L. Green; J.Nucl.Matter. 105 (1982) 1.

[3] M. Victoria, W.V. Green, B.N. Singh, and T. Leffers; J.Nucl. Mater. 122 & 123 (1984) 737.

[4] D. Gavillet, Ph.D. Thesis No. 652, Ecole Polytechnique Fédérale de Lausanne, Switzerland, October 1986.

[5] F. Paschoud, R. Gotthardt, D. Gavillet, W.V. Green, and M. Victoria; "The Growth of Bubbles and Precipitates in Pure Aluminium During and After Irradiation with 590 MeV Protons". Presented in the Symposium on the Effects of Radiation on Materials, Andover, Mass. USA, June 1988.

[6] F. Paschoud, R. Gotthardt, and S.L. Green in "Radiation Induced Changes in Microstructure: 13th International Symposium" ASTM STP 955, F.A Garner, N.H. Packan and A.S. Kumar, Eds., 1987, pp. 478 – 489.

[7] J.K. Kjems, B.N Singh, B. Sjoberg, M. Victoria, and S.L. Green in "Microstructural Characterization of Materials by Non-Microscopical Techniques"; N.H. Andersen et al. Eds., Risø, Denmark, (1984).

[8] K.O. Jensen, B.N. Singh, M. Eldrup, M. Victoria, and W.V. Green in ref. [7], p. 333.

[9] K.O. Jensen, M. Eldrup, B.N. Singh, A. Horsewell, M. Victoria, and W.F. Sommer; Materials Science Volumes 15-18 (1987) 913.

[10] D. Gavillet, W.V. Green, M. Victoria, and J.L. Martin; Rad.Effects 101 (1986) 269.

[11] D. Gavillet, W.V. Green, M. Victoria, R. Gotthardt, and J.L. Martin in ref. [6], pp. 490 - 497.

[12] D. Gavillet, M. Victoria, W.V. Green, R. Gotthardt, and J.L. Martin; J.Nucl.Mater. 155-157 (1988) 992.

[13] W.A. Coleman, and T.W. Armstrong; Report ORN 64606 (1970), Oak Ridge National Laboratory, USA.

[14] S.L. Green; J.Nucl.Mater. 126 (1984) 30.

[15] R. Serber; Phys.Rev. 72 (1947) 1114.

[16] M.T. Robinson in "Radiation Induced Voids in Metals", J.W. Corbett, and L.C. Iannello, Eds. CONF - 710601, National Technical Information Service, USA, 1972, pp. 397 - 429.

[17] J. Lindhard, V. Nielsen and M. Sharff; K. Dan. Videsk. Selsk., Mat.-Fys.Med. 10 (1968) 36.

[18] C. Ponti; MANET-2 in NET.DN, ISPRA, private communication, 1987.

[19] M. Huggenberger, EIR Technical Note TM-23-83-12 (1983); Technical Note AN-23-84-10, (1984); M. Huggenberger, and H. Nöthiger, Technical Note TM-23-84-18, (1984); H. Nöthiger, Technical Note AN- 23-85-06, (1985); H. Nöthiger, Technical Note TM-23-85-06, (1985); H. Nöthiger, and M. Huggenberger, Technical Note TM-23-86-02, (1986); H. Nöthiger, Technical Note TM-23-87-09, (1987).

[20] S.L. Green, W.V. Green, F.HG. Hegedus, M. Victoria, W.F. Sommer, and B.M. Oliver, Production of Helium by Medium Energy Protons; J.Nucl.Mat. 155-157 (1988) 1350.